Order online now!

www.rockland.com
tech@rockland.com
+1 484.791.3823

Datasheet for 600-301-215

# GFP Monoclonal Antibody

## Overview

| | |
|---|---|
| **Description:** | Anti-GFP (MOUSE) Monoclonal Antibody - 600-301-215 |
| **Item No.:** | 600-301-215 |
| **Size:** | 1 mg |
| **Applications:** | Dot Blot, ELISA, IP, WB, ChIP, EM, FC, IF, IHC, Multiplex |
| **Reactivity:** | GFP, eGFP, rGFP |
| **Host Species:** | Mouse |

## Product Details

| | |
|---|---|
| **Background:** | Green fluorescent protein is a 27 kDa protein produced from the jellyfish Aequorea victoria, which emits green light (emission peak at a wavelength of 509nm) when excited by blue light. GFP is an important tool in cell biology research. GFP is widely used enabling researchers to visualize and localize GFP-tagged proteins within living cells without the need for chemical staining. |
| **Synonyms:** | mouse anti-GFP antibody, Green Fluorescent Protein, GFP antibody, Green Fluorescent Protein antibody, EGFP, enhanced Green Fluorescent Protein, Aequorea victoria, Jellyfish |
| **Host Species:** | Mouse |
| **Clonality:** | Monoclonal |
| **Clone ID:** | 9F9.F9 |
| **Format:** | IgG |

## Target Details

| | |
|---|---|
| **Reactivity:** | GFP, eGFP, rGFP |
| **Immunogen Type:** | Recombinant Protein |
| **Immunogen:** | Recombinant Green Fluorescent Protein (GFP) fusion protein corresponding to the full length amino acid sequence (246 aa) derived from the jellyfish Aequorea victoria. |

| | |
|---|---|
| **Purity/Specificity:** | GFP Monoclonal Antibody was prepared from tissue culture supernatant by Protein A affinity chromatography. Assay by Immunoelectrophoresis resulted in a single precipitin arc against anti-Mouse Serum. Reactivity is observed against recombinant Green Fluorescent Protein (000-001-215) from Aequorea victoria by both Western blot and ELISA. No reaction is seen against RFP. |
| **Relevant Links:** | • UniProtKB - P42212 |

## Application Details

| | |
|---|---|
| **Tested Applications:** | Dot Blot, ELISA, IP, WB |
| **Suggested Applications:** | ChIP, EM, FC, IF, IHC, Multiplex (Based on references) |
| **Application Note:** | Monoclonal anti-GFP is designed to detect enhanced GFP and GFP containing recombinant proteins. Tested in ELISA, IP, and WB and suitable in FACS, IHC, IF. This antibody can be used to detect GFP by ELISA (sandwich or capture) for the direct binding of antigen. Biotin conjugated monoclonal anti-GFP is well suited to titrate GFP in a sandwich ELISA in combination with Rockland's polyclonal anti-GFP (600-101-215) as the capture antibody. Only use the monoclonal form for the detection of enhanced or recombinant GFP. Polyclonal anti-GFP detects all variants of GFP tested to date. The biotin conjugated detection antibody is typically used with streptavidin conjugated HRP (code # S000-03) or other streptavidin conjugates. The use of polyclonal anti-GFP results in significant amplification of signal when fluorochrome conjugated polyclonal anti-GFP is used relative to the fluorescence of GFP alone. For immunoblotting use either alkaline phosphatase or peroxidase conjugated anti-GFP to detect GFP or GFP containing proteins on western blots. Optimal titers for applications should be determined by the researcher. |
| **Assay Dilutions:** | All assays should be optimized by the user. Recommended dilutions (if any) may be listed below. |
| **ELISA:** | 1:10,000 - 1:30,000 |
| **FC:** | User Optimized |
| **IF:** | User Optimized |
| **IHC:** | 1:1,000 - 1:5,000 |
| **WB:** | 1:3,000 - 1:30,000 |

## Formulation

| | |
|---|---|
| **Physical State:** | Liquid (sterile filtered) |
| **Concentration:** | 1.0 mg/mL by UV absorbance at 280 nm |
| **Buffer:** | 0.02 M Potassium Phosphate, 0.15 M Sodium Chloride, pH 7.2 |

| | |
|---|---|
| **Preservative:** | 0.01% (w/v) Sodium Azide |
| **Stabilizer:** | None |

## Shipping & Handling

| | |
|---|---|
| **Shipping Condition:** | Dry Ice |
| **Storage Condition:** | Store mouse anti-GFP at -20° C prior to opening. Aliquot contents and freeze at -20° C or below for extended storage. Avoid cycles of freezing and thawing. Centrifuge product if not completely clear after standing at room temperature. This product is stable for several weeks at 4° C as an undiluted liquid. Dilute only prior to immediate use. |
| **Expiration:** | Expiration date is one (1) year from date of receipt. |

## Images

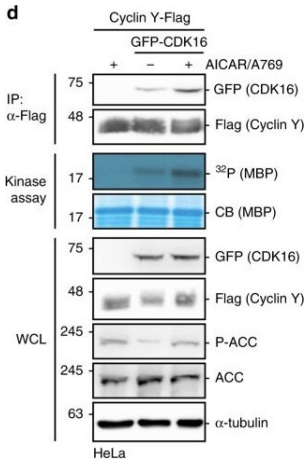


**Western Blot**

Protein microarray screen for the identification of AMPK substrates.a Schematic representation of the ProtoArray based screen with approximately 9000 human proteins using AMPK (see also Supplementary Data 1). b Details of two sub-arrays incubated with or without AMPK with marked substrates are shown. c GST-CDK16, Cyclin Y-His6 and GST were incubated in the presence of [γ-32P]-ATP with AMPK. Phosphorylation was determined by autoradiography (32P, top). Proteins were visualized by Coomassie blue staining (CB, bottom; n = 2). d HeLa cells were transfected with vectors expressing GFP-CDK16 and Cyclin Y-Flag and treated for 1 h with 0.5 mM AICAR/50 µM A769662 (A769) as indicated. Cyclin Y-Flag was immunoprecipitated with Flag antibodies (IP) and immunoblotted against CDK16 and Cyclin Y or used for in vitro kinase assays with myeloid basic protein (MBP) as substrate. Autoradiographs (32P) and Coomassie blue staining (CB) of MBP are displayed. Whole cell lysates (WCL) were immunoblotted with the indicated antibodies (n = 3). e Quantification of CDK16 co-immunoprecipitated with Cyclin Y. Statistical significance was measured via unpaired and two-tailed Student's t-tests and is presented as follows: **p < 0.01, and ***p < 0.001. All error bars indicate SD (n = 3; Cyclin Y + AICAR/A769 vs. Cyclin Y/CDK16: t = 8.719, df = 4; Cyclin Y/CDK16 vs. Cyclin Y/CDK16 + AICAR/A769: t = 5.595, df = 4). n biological independent replicate. SD standard deviation. Source data are provided as a Source Data file. Figure provided by CiteAb. Source: Nat Commun, PMID: 32098961.

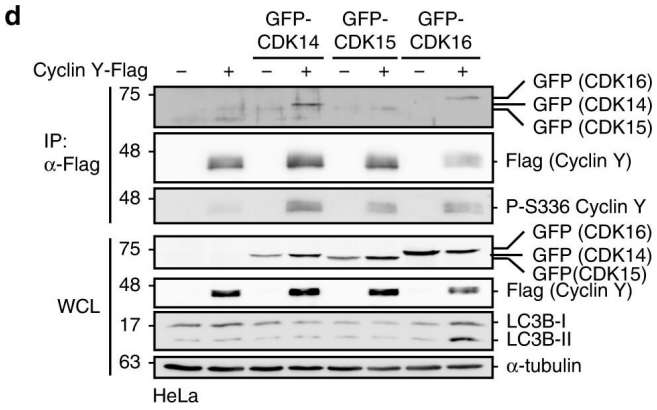


**Western Blot**

Active Cyclin Y/CDK16 complexes induce autophagy.a NIH3T3 cells stably expressing mCherry-GFP-LC3 were transfected with HA-CDK16 and Cyclin Y-Flag as indicated or treated for 2 h with EBSS or for 4 h with 200 nM Bafilomycin A1 (Baf. A1) and lysates were immunoblotted as indicated. KR kinase-deficient CDK16 mutant, AA CDK16 binding deficient Cyclin Y mutant (n = 3). b Representative confocal images of the NIH3T3-mCherry-GFP-LC3 cells treated as in panel a. Staining of the HA-CDK16 in purple identified transfected cells. Autophagosomes (yellow dots) and autolysosomes (red dots) were detected by an overlay of the GFP and mCherry fluorescent signals. Scale bar: 20 µm. c Quantification of autophagosomes (yellow dots) and autolysosomes (red dots) of cells shown in panel b. Statistical significance was measured via unpaired and two-tailed Student's t-tests and is presented as follows: **p < 0.01. All error bars indicate SD (n = 3; 50 cells counted for each replicate; wt vs. KR: t = 5.707, df = 4; wt vs. AA: t = 5.557, df = 4). d GFP-tagged CDK14, CDK15 or CDK16 were expressed with or without Cyclin Y-Flag in HeLa cells. Cyclin Y was immunoprecipitated with a Flag antibody (IP). Lysates were immunoblotted with the indicated antibodies (WCL). (n = 4) e Representative confocal images of HeLa cells treated as in panel d. Fluorescent GFP signals identified CDK expressing cells. Endogenous LC3 (red) was used to measure autophagy with the 4E12 antibody. Scale bar: 50 µm. f Quantification of the LC3 dots shown in panel e. Statistical significance was measured via unpaired and two-tailed Student's t-tests and is presented as follows: ****p < 0.0001. All error bars indicate SD. (n = 1; 100 cells were counted for each treatment; control vs. Cyclin Y/CDK16: t = 6.771, df = 14; Cyclin Y/CDK14 vs. Cyclin Y/CDK16: t = 6.855, df = 14; Cyclin Y/CDK15 vs. Cyclin Y/CDK16: t = 7.139, df = 15). n biological independent replicate. SD standard deviation. Source data are provided as a Source Data file. Figure provided by CiteAb. Source: Nat Commun, PMID: 32098961.

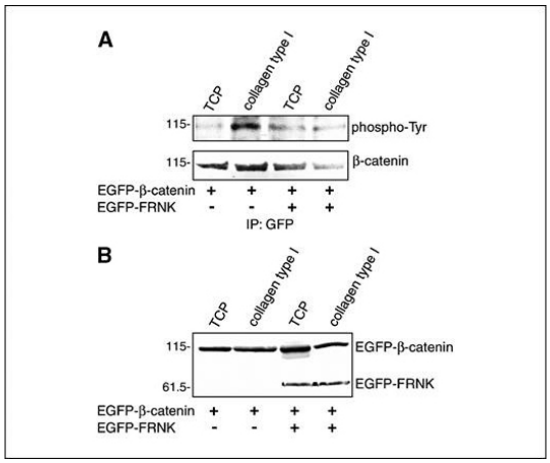


**Western Blot**

FAK-dependent phosphorylation of β-catenin. A, the influence of FAK on tyrosine phosphorylation of β-catenin was investigated by expression of the EGFP-tagged kinase-deficient FAK mutant FRNK. EGFP-β-catenin (lanes 1 and 2) or EGFP-β-catenin and EGFP-FRNK (lanes 3 and 4) were transfected into Panc-1 cells cultivated on TCP (lanes 1 and 3) or type I collagen (lanes 2 and 4). Immunoprecipitation of EGFP-tagged transfected proteins was done with anti-GFP antibody (p/n 600-301-215) from 0.5 mg of total lysate. Tyrosine phosphorylation of the precipitates were analyzed by immunoblotting with a phosphotyrosine-specific antibody. EGFP-tagged β-catenin was identified by its apparent molecular weight (protein plus EGFP-tag) and verified by re-staining with anti-β-catenin antibody. B, to verify proper expression of transfected proteins, 50 µg of cell lysates from Panc-1 cells transfected with EGFP-β-catenin (lanes 1 and 2) or EGFP-β-catenin and EGFP-FRNK were immunoblotted using an anti-GFP antibody (p/n 600-301-215). Fig 4. PMID: 16651417

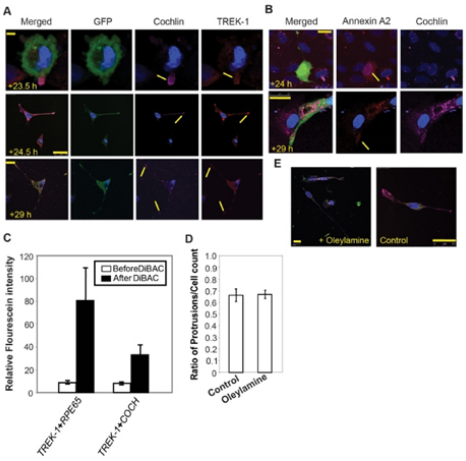


**Immunofluorescence Microscopy**

(A) Immunocytochemical analysis of cells expressing cochlin and green fluorescence protein (GFP). The cells were imaged at 23.5, 24.5 and 29 hours post-transfection as indicated and probed for TREK-1 (red), GFP (green) and cochlin (pink). Arrows show localization of cochlin and TREK-1 in the filopodia. Scale bar, 5 µm (top panel), 50 µm (middle panel), 25 µm (bottom panel). (B) Immunocytochemical analysis of cells expressing cochlin and GFP. The cells were imaged at 24 and 29 hours post-transfection as indicated and probed for annexin A2 (red) and cochlin (pink). Scale bar, 25 µm. (C) Comparison of relative fluorescein intensity in the TM cells transfected with TREK-1+ RPE65 and TREK-1+COCH before and after the addition of DiBAC as indicated. Results from five different experiments are shown (mean ± SD). (D) Comparison of filopodia induction in the cells cultured in the presence or absence of oleylamine (5 µM). Results from three different experiments are shown (mean ± SD). (E) Representative images of cells expressing cochlin and GFP when grown in the presence or absence of oleylamine (5 µM) as indicated. Scale bar, 50 µm. In all sections nuclei were stained with DAPI.
Fig 2. PMID: 21886777

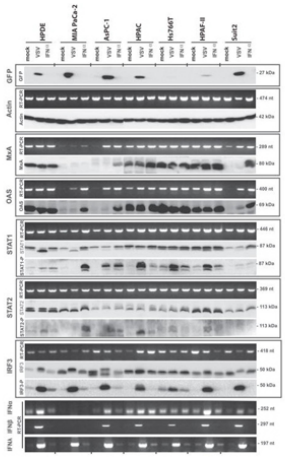

**Western Blot**
Cells were mock infected, infected with VSV-ΔM51-GFP (indicated as VSV) at MOI 10 CIU/cell or treated with 5,000 U/ml IFN-α. Cells were harvested at 12 h p.i. and mRNA was reverse transcribed and analyzed by semi-quantitative PCR or cell lysates were prepared and analyzed by western blot for the indicated protein. PCR (nt) and protein (kDa) product sizes are indicated on the right. Fig 2.
PMID: 23246628

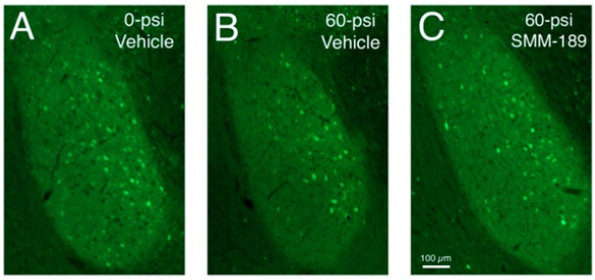


**Immunofluorescence Microscopy**
Images of sections through the basolateral amygdala on the blasted side from mice engineered to express enhanced yellow fluorescent protein (EYFP) in Thy1-enriched telencephalic neurons. Note that the basolateral amygdala (BLA) in the vehicle-treated 0-psi mouse (A) contains numerous Thy1-EYFP+ neurons, while the BLA in the vehicle-treated 50-psi mouse (B) contains fewer. Thy1+ neurons in BLA are increased in SMM-189-treated 50-psi mice (C) above that seen in the vehicle-treated 50-psi mouse. Immunolabeling for GFP (p/n 600-301-215) using the PAP method was used to render EYFP detectible by transmitted light microscopy. Fig 12. PMID: 25561230

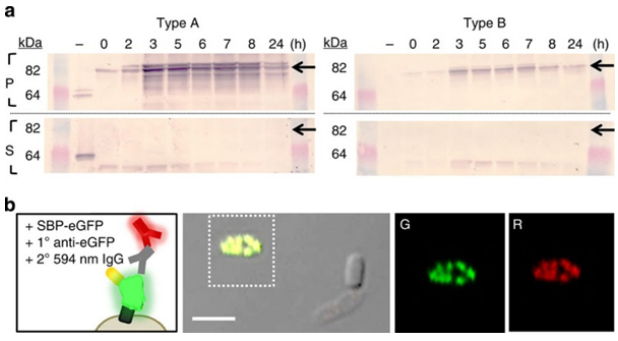


**Immunofluorescence Microscopy**
64–82 kDa region of western blot for pelleted (P) and supernatant (S) protein fractions isolated from Type A and B cells. Alkaline phosphatase-conjugated streptavidin was used to target AIDAc–Venus–SBP at expression timepoints. Arrows indicate the expected position of the full fusion protein. (b) Immunostaining for assessment of the fluorescent protein surface accessibility. The external surfaces of cells expressing AIDAc–eGFP–SBP were probed with an anti–eGFP (p/n 600-301-215) and Alexafluor594-labelled antibody pair. A representative overlaid fluorescence and phase contrast image is shown along with fluorescence images of the green (G) and red (R) filters for the boxed-in region. Scale bar, 2 µM. Fig 4.
PMID: 26455828

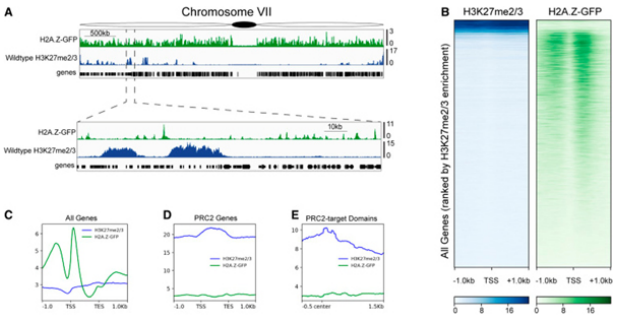


**ChIP**

H3K27me2/3 and H2A.Z are not colocalized in N. crassa mycelium. (A) Genome browser images of ChIP-seq for H2A.Z-GFP (green) and H3K27me2/3 (blue) enrichment across Linkage Group ("chromosome") VII. A segment of chromosome VII is displayed at higher resolution to visualize the distinct patterns of each modification. Distinct peaks are located at the start of many genes in the genome yet few H2A.Z peaks are present within transcriptionally silent PRC2-target domains. (B) Heatmaps of H3K27me2/3 (blue) and H2A.Z-GFP (green) enrichment ordered by H3K27me2/3 enrichment. Heatmaps are centered on the transcription start site (TSS) for all 10,397 genes, + or –1000 bp for a full window size of 2000 bp. (C) Gene profile of H2A.Z-GFP (green line) and H3K27me2/3 (blue line) enrichment for all 10,397 genes (fit to 1000 bp for gene body length) in the genome –1000 bp upstream of TSS, and +1000 bp downstream of TES. (D) Gene profile of H2A.Z-GFP (green line) and H3K27me2/3 (blue line) enrichment for only H3K27me2/3 genes (589 genes) enriched in the genome –1000 bp upstream of TSS and + 1000 bp downstream of TES. (E) Line plot centered on 325 PRC2-target domains displays very low enrichment for H2A.Z-GFP (green line) and high enrichment for H3K27me2/3 (blue line). Fig 3.
PMID: 32651262

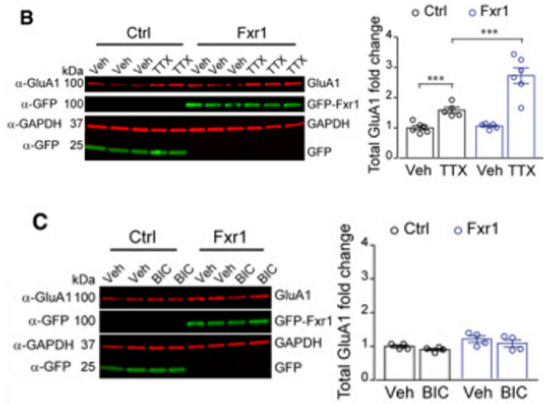


**Western Blot**

(B) Western blot analysis of total GluA1 expression in Ctrl or Fxr1 overexpression (Fxr1) condition during upscaling (Ctrl/Veh n = 5, Ctrl/TTX n = 5, Fxr1/Veh n = 6, Fxr1/Veh n = 6). One-way ANOVA with Dunnett's multiple comparison test ***P < 0.001.
(C) Western blot analysis of total GluA1 expression in Ctrl or Fxr1 over condition during downscaling (Ctrl/Veh n = 4, Ctrl/TTX n = 4, Fxr1/Veh n = 4, Fxr1/Veh n = 4).
Fig 2. PMID: 32893934

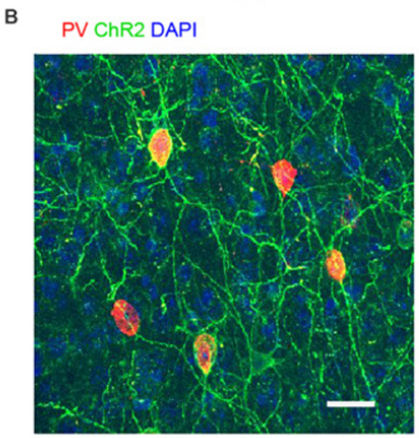


**Immunofluorescence Microscopy**
(B) Immunostaining of PV (red), EYFP (green) and DAPI (blue) confirmed the co-localization of PV and ChR2 in the PFC of PV-ChR2-EYFP transgenic mice. Scale: 50 µm. Fig 1.
PMID: 33324170

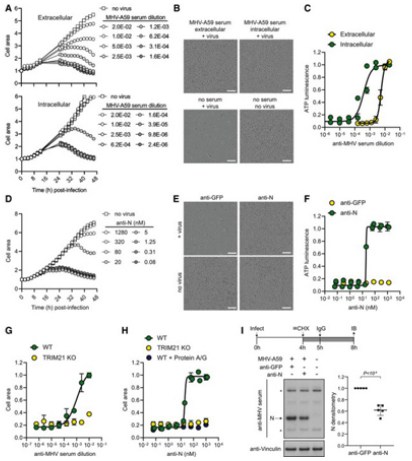

**Western Blot**

A) A titration of anti-MHV polyclonal serum was added either directly to media (extracellular) or electroporated into L929 cells (intracellular), and then, cells were infected with MHV-A59. The kinetics of cell growth was monitored by measuring total cell area.

B) Phase-contrast images of cells at 48 h post-infection. Scale bar = 200 µm.

C) At 48 h post-infection, the viability of cells infected with MHV-A59 in the presence of intracellular or extracellular antiserum was determined by ATP luminescence assay. Increasing doses of antiserum results in increased cell survival.

D) Kinetics of cell growth following MHV-A59 infection in the presence of a titration of electroporated anti-N antibody.

E) Phase-contrast images of cells at 48 h post-infection. Scale bar = 200 µm.

F) Quantification of cell viability by ATP luminescence assay at 48 h post-infection in the presence of electroporated anti-N or anti-GFP antibodies.

G, H) WT or TRIM21 KO L929 cells were infected with MHV-A59 in the presence of electroporated polyclonal antiserum (G) or anti-N antibody (H) and quantified by cell area 48 h later. Co-electroporation of protein A/G with anti-N antibody into WT cells mimics the TRIM21 KO phenotype.

I) L929 cells were infected with MHV-A59 for 4 h, and then, cyclohexamide (CHX) was added to block further viral protein synthesis. After 5 h, cells were electroporated with anti-N or anti-GFP antibodies and left for a further 3 h before being western blotted for cellular N protein levels (* denotes a non-specific band).

Data information: Data were analysed using a Student's t-test. Error bars depict the mean +/- SEM. All data represent at least two independent replicates. Fig 1.

PMID: 34323299

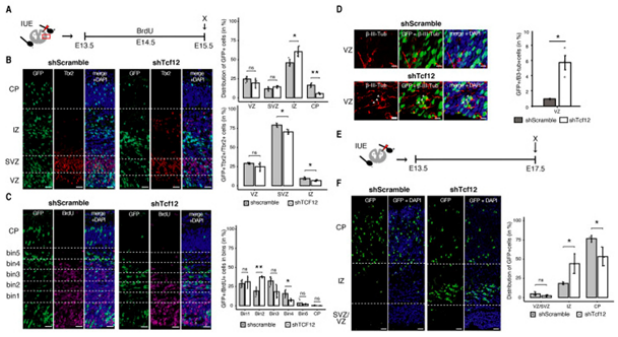

**Immunofluorescence Microscopy**

Loss of Tcf12 impairs neuronal migration during cortical development. (A) Experimental layout for the in utero electroporation (IUE) assay where IUE was carried out at E13.5 and analysed at E15.5. (B) Immunofluorescence images showing phenotypic changes following depletion of Tcf12. Here, E15.5 cortex electroporated at E13.5 with a control shscramble or a shTcf12 plasmid containing a GFP reporter (left panel) was analysed for the distribution of GFP + and GFP+ Tbr2+/Tbr2+ cells (in %) across the cortical layers (right panel). (C) Neuronal migration was assessed by identifying five equidistant bins across the SVZ/IZ (left panel) and quantifying the distribution of GFP+/BrDU+ population (in %) in these bins (right panel). (D) Immunofluorescence images showing the expression of the neuron-specific marker β-III-Tubulin upon Tcf12 knockdown (left panel) and the distribution of GFP+/β-III-Tub+ cells (in %) in the ventricular zone (VZ) (right panel). (E) Experimental schematic for the in utero electroporation (IUE) assay where IUE was carried out at E13.5 and analysed at E17.5. (F) Immunofluorescence images showing phenotypic changes in the developing cortex following a prolonged knockdown of Tcf12 (left panel). The distribution of electroporated cortical cells (GFP+ cells) across the cortical layers is shown (in %) (right panel). Scale bars: 100 µm. Statistical significance was calculated using an unpaired two-tailed Student's t-test. *P<0.05, **P<0.01; n=3 or 4 independent biological replicates. Data are mean±s.d. Fig 5. PMID: 35147187

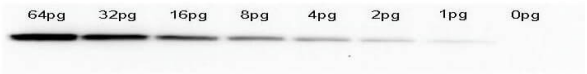


**Dot Blot**

Western Blot of anti-GFP monoclonal antibody. Lane 1: 64pg of recombinant GFP protein (p/n 000-001-215) were spiked into a HeLa cell-derived lysates (p/n W09-000-364). Lane 2: 32pg of recombinant GFP protein were spiked into a HeLa cell-derived lysates. Lane 3: 16pg of recombinant GFP protein were spiked into a HeLa cell-derived lysates. Lane 4: 8pg of recombinant GFP protein were spiked into a HeLa cell-derived lysates. Lane 5: 4pg of recombinant GFP protein were spiked into a HeLa cell-derived lysates. Lane 6: 2pg of recombinant GFP protein were spiked into a HeLa cell-derived lysates. Lane 7: 1g of recombinant GFP protein were spiked into a HeLa cell-derived lysates. Lane 8: 0pg of recombinant GFP protein were spiked into a HeLa cell-derived lysates. Primary antibody: anti-GFP monoclonal antibody at 1:400 for overnight at 4°C. Secondary antibody: HRP-conjugated anti-Mouse IgG (p/n 610-4302) was performed at a dilution of 1:20,000 for 1h at 4°C. Block: TTBS (p/n MB-013) supplemented with 1% BSA (p/n BSA-50) for 1 h at 4°C. Predicted/Observed size: 27 kDa for GFP. Other band(s): none.

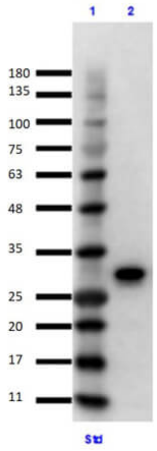


**Western Blot**

Immunoprecipitation/Western Blot using GFP Protein. Lane 1: Opal Prestained Molecular Weight Marker (p/n MB-210-0500). Lane 2: GFP Input (p/n 000-001-215) Reduced [10µL]. Primary IP Antibody: Mouse Anti-GFP (p/n 600-301-215) at 10µg overnight at 2-8°C. Secondary Antibody: TrueBlot Anti-Mouse Ig IP Agarose Beads (p/n 00-8811-25) at 500µg for 1hr at RT. Buffer: BlockOut Buffer (p/n MB-073) for 30 mins at RT. Exposure: 7 sec.

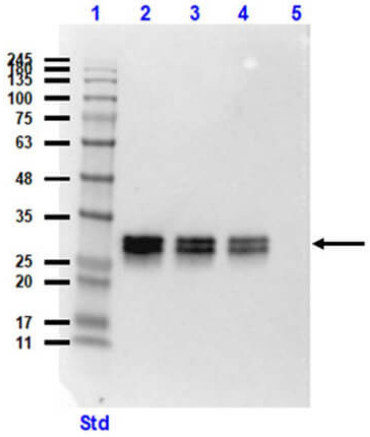


**Western Blot**
Western blot of Mouse Anti-GFP Antibody. Lane 1: Opal Prestained Molecular Weight Marker (p/n MB-210-0500). Lane 2: HeLa WC Lysate+GFP protein (p/n W09-000-364 [10µg]/ p/n 000-001-215 [50ng]). Lane 3: HeLa WC Lysate +GFP protein (10µg/20ng). Lane 4: HeLa WC Lysate+GFP protein (10µg/10ng). Lane 5: HeLa Whole Cell Lysate (p/n W09-000-364) (10µg). Primary Antibody: Anti-GFP at 1:1000 overnight at 2-8°C. Secondary Antibody: Rabbit Anti-Mouse IgG HRP (p/n 610-4302) at 1:40,000 for 30mins at RT. Block: BlockOut Buffer (p/n MB-073). Expected MW: ~27kDa.

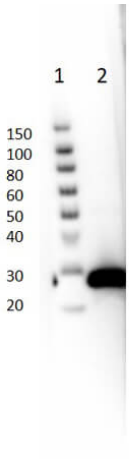


**Western Blot**
Western blot of Mouse Anti-GFP Antibody. Lane 1: Thermo SuperSignal Molecular Weight Marker. Lane 2: GFP protein (p/n 000-001-215) [50ng]. Primary Antibody: Anti-GFP at 1:1000 overnight at 2-8°C. Secondary Antibody: Rabbit Anti-Mouse IgG HRP (p/n 610-4302) at 1:40,000 for 30mins at RT. Block: BlockOut Buffer (p/n MB-073). Expected MW: ~27kDa.

## References


- Shaw L et al. Projection-specific intersectional optogenetics for precise excitation and inhibition in the marmoset brain. *Cell Rep Methods.* (2026)
- Hu Y et al. SHANK3 mutations disrupt olfactory valence coding across species, with cortical amygdala mechanisms identified in mice. *Sci Adv.* (2026)
- Châtel-Soulet HÉ et al. Thrombopoietin increases susceptibility for EVI1 + KMT2A-MLLT3-driven AML expressing stem cell genes linked to poor outcome. *Nat Commun.* (2025)
- Lin X et al. XRCC1 mediates PARP1- and PAR-dependent recruitment of PARP2 to DNA damage sites. *Nucleic Acids Res.* (2025)
- Huang L et al. Assay development and validation for innovative antiviral development targeting the N-terminal autoprocessing of SARS-CoV-2 main protease precursors. *Viruses.* (2024)

- Singh, A et al. Tcf12 and NeuroD1 cooperatively drive neuronal migration during cortical development. *Development (Cambridge, England)* (2022)
- Albecka A et al. A functional assay for serum detection of antibodies against SARS-CoV-2 nucleoprotein. *EMBO J.* (2021)
- Kumar S et al. The neural G protein Gαo tagged with GFP at an internal loop is functional in Caenorhabditis elegans. *G3 (Bethesda).* (2021)
- Dohmen M et al. AMPK-dependent activation of the Cyclin Y/CDK16 complex controls autophagy. *Nat Commun.* (2020)
- Garg T. et al. Genome-Wide High Resolution Expression Map and Functions of Key Cell Fate Determinants Reveal the Dynamics of Crown Root Development in Rice. *bioRxiv.* (2020)
- Sundaramurthy S. et al. FHOD-1 is the only formin in Caenorhabditis elegans that promotes striated muscle growth and Z-line organization in a cell autonomous manner. *Cytoskeleton (Hoboken).* (2020)
- Santos M et al. Novel MAG Variant Causes Cerebellar Ataxia with Oculomotor Apraxia: Molecular Basis and Expanded Clinical Phenotype. *J Clin Med.* (2020)
- Zaja R et al. Comparative analysis of MACROD1, MACROD2 and TARG1 expression, localisation and interactome. *Sci Rep.* (2020)
- Courtney AJ et al. Normal Patterns of Histone H3K27 Methylation Require the Histone Variant H2A.Z in Neurospora crassa. *Genetics.* (2020)
- Khlghatyan J et al. Fxr1 regulates sleep and synaptic homeostasis. *EMBO J.* (2020)
- Tian Y et al. The mono-ADP-ribosyltransferase ARTD10 regulates the voltage-gated K+ channel Kv1. 1 through protein kinase C delta. *BMC Biol.* (2020)
- Yao Y et al. Phase Coupled Firing of Prefrontal Parvalbumin Interneuron With High Frequency Oscillations. *Front Cell Neurosci.* (2020)
- Santos M, Morais S, Pereira C, Sequeiros J, Alonso I. Parkin truncating variants result in a loss-of-function phenotype. *Sci Rep.* (2019)
- Brito, C et al. Perfringolysin O-Induced Plasma Membrane Pores Trigger Actomyosin Remodeling and Endoplasmic Reticulum Redistribution. *Toxins* (2019)
- Liu, W et al. Alp7-Mto1 and Alp14 synergize to promote interphase microtubule regrowth from the nuclear envelope. *Journal of Molecular Cell Biology* (2019)
- Nicholson DA, Roberts TF, Sober SJ. et al. Thalamostriatal and cerebellothalamic pathways in a songbird, the Bengalese finch. *J Comp Neurol.* (2018)
- Khlghatyan et al. Mental Illnesses-Associated Fxr1 and Its Negative Regulator Gsk3β Are Modulators of Anxiety and Glutamatergic Neurotransmission. *Frontiers in Molecular Neuroscience* (2018)
- Swiatkowski P et al. Role of Akt-independent mTORC1 and GSK3β signaling in sublethal NMDA-induced injury and the recovery of neuronal electrophysiology and survival. *Sci Rep.* (2017)
- Terrell et al. Nano-guided cell networks as conveyors of molecular communication. *Nature Communications* (2015)
- Reiner, A et sl. Motor, visual and emotional deficits in mice after closed-head mild traumatic brain injury are alleviated by the novel CB2 inverse agonist SMM-189. *International Journal of Molecular Sciences* (2014)

- Sebastian, K et al. Characterization of SLCO5A1/OATP5A1, a solute carrier transport protein with non-classical function. *PloS One* (2013)
- Moerdyk-Schauwecker M et al. Resistance of pancreatic cancer cells to oncolytic vesicular stomatitis virus: role of type I interferon signaling. *Virology.* (2013)
- Feijs KL et al. ARTD10 substrate identification on protein microarrays: regulation of GSK3β by mono-ADP-ribosylation. *Cell Commun Signal.* (2013)
- Forst AH et al. Recognition of mono-ADP-ribosylated ARTD10 substrates by ARTD8 macrodomains. *Structure.* (2013)
- Hastie E et al. Oncolytic vesicular stomatitis virus in an immunocompetent model of MUC1-positive or MUC1-null pancreatic ductal adenocarcinoma. *J Virol.* (2013)
- Vladimir A Volkov et al. Long tethers provide high-force coupling of the Dam1 ring to shortening microtubules. *Proc Natl Acad Sci U S A.* (2013)
- Goel M et al. Cochlin, Intraocular Pressure Regulation and Mechanosensing. *PLoS One.* (2012)
- Goel M et al. Cochlin induced TREK-1 co-expression and annexin A2 secretion: role in trabecular meshwork cell elongation and motility. *PLoS One.* (2011)
- Jesse S et al. Lef-1 isoforms regulate different target genes and reduce cellular adhesion. *Int J Cancer.* (2010)
- Zanger RC et al. ProMAT Calibrator: a tool for reducing experimental bias in antibody microarrays. *J Proteome Res.* (2009)
- Koenig A et al. Collagen Type I Induces disruption of E-cadherin–mediated cell-cell contacts and promotes proliferation of pancreatic carcinoma cells. *Cancer Res.* (2006)


## Disclaimer